Biosensors and Bioelectronics 141 (2019) 111361

Contents lists available at ScienceDirect

Biosensors and Bioelectronics

journal homepage: www.elsevier.com/locate/bios

Use of anti-CRISPR protein AcrIIA4 as a capture ligand for CRISPR/Cas9 detection

Robert K. Johnston[a], Kyle J. Seamon[b], Edwin A. Saada[b], Joshua D. Podlevsky[c], Steven S. Branda[c], Jerilyn A. Timlin[c,**], Jason C. Harper[c,*]

[a] Nanobiology Department, Sandia National Laboratories, Albuquerque, NM, USA
[b] Systems Biology Department, Sandia National Laboratories, Livermore, CA, USA
[c] Bioenergy and Defense Technologies, Sandia National Laboratories, Albuquerque, NM, USA

ARTICLE INFO

Keywords:
CRISPR/Cas9
Anti-CRISPR protein
Affinity reagent
Electrochemistry

ABSTRACT

The clustered regularly interspaced short palindromic repeats (CRISPR)/CRISPR-associated protein 9 (Cas9) ribonucleoprotein (RNP) complex is an RNA-guided DNA-nuclease that is part of the bacterial adaptive immune system. CRISPR/Cas9 RNP has been adapted for targeted genome editing within cells and whole organisms with new applications vastly outpacing detection and quantification of gene-editing reagents. Detection of the CRISPR/Cas9 RNP within biological samples is critical for assessing gene-editing reagent delivery efficiency, retention, persistence, and distribution within living organisms. Conventional detection methods are effective, yet the expense and lack of scalability for antibody-based affinity reagents limit these techniques for clinical and/or field settings. This necessitates the development of low cost, scalable CRISPR/Cas9 RNP affinity reagents as alternatives or augments to antibodies. Herein, we report the development of the *Streptococcus pyogenes* anti-CRISPR/Cas9 protein, AcrIIA4, as a novel affinity reagent. An engineered cysteine linker enables covalent immobilization of AcrIIA4 onto glassy carbon electrodes functionalized *via* aryl diazonium chemistry for detection of CRISPR/Cas9 RNP by electrochemical, fluorescent, and colorimetric methods. Electrochemical measurements achieve a detection of 280 pM RNP in reaction buffer and 8 nM RNP in biologically representative conditions. Our results demonstrate the ability of anti-CRISPR proteins to serve as robust, specific, flexible, and economical recognition elements in biosensing/quantification devices for CRISPR/Cas9 RNP.

1. Introduction

Clustered regularly interspaced short palindromic repeats (CRISPR) and the CRISPR associated system (Cas) form a bacterial and archaeal adaptive immune system that utilizes targeted nucleases to identify and destroy invading mobile genetic elements (Barrangou et al., 2007; Datsenko et al., 2012; Barrangou and Marraffini, 2014). The effector molecule is a ribonucleoprotein (RNP) complex comprised of one or more nucleolytic Cas proteins and a guide RNA specific for the invading genetic element. The RNP scans for nucleic acids complementary to the guide RNA, cleaving them when a threshold level of base pair binding between the target molecule and the guide RNA is achieved. In 2012, Jinek et al. showed that an engineered single guide RNA (sgRNA) in combination with Cas from *Streptococcus pyogenes* (SpyCas9) could introduce double stranded breaks (DSBs) at desired sequences in DNA *in vitro* (Jinek et al., 2012). Subsequent studies using SpyCas9 in living cells showcased the profound potential for efficient, targeted genome editing afforded by CRISPR/Cas systems.

In developing CRISPR/Cas systems as gene editing tools, including those designed for therapeutic use, researchers and clinicians have come to appreciate that quantifying CRISPR/Cas delivery, persistence, and activity in complex sample matrices (*e.g.*, cell lysates, blood, specimens) is vital for establishing and optimizing pharmacokinetic and pharmacodynamic profiles for CRISPR/Cas-mediated therapeutic editing, as well as for minimizing risk of deleterious off-target editing and immune system activation (Pattanayak et al., 2013; Charlesworth et al., 2018; Chew, 2018; Crudele and Chamberlain, 2018; Wagner et al., 2019). Currently, protein detection methods (*e.g.*, Western analysis, ELISA) rely on anti-Cas antibodies for CRISPR/Cas system recognition and detection. While effective, the expense and scalability of antibody reagents potentially limits the applicability of these detection methods to small scale laboratory and clinical settings. Developing

* Corresponding author.
** Corresponding author.
E-mail address: jcharpe@sandia.gov (J.C. Harper).

https://doi.org/10.1016/j.bios.2019.111361
Received 14 March 2019; Received in revised form 25 May 2019; Accepted 28 May 2019
Available online 31 May 2019
0956-5663/

lower cost, more scalable CRISPR/Cas affinity reagents that can replace, or augment, antibodies in detection platforms is therefore necessary for utility in large scale laboratory, clinical, and field settings.

Fortuitously, nature has provided a deep pool of potential biomolecular affinity reagents in the form anti-CRISPR (Acr) proteins First discovered by Bondy-Denomy et al. (Bondy-Denomy et al., 2013; Pawluk et al., 2014), Acr proteins are produced by bacteriophage, enabling them to inhibit CRISPR/Cas and thereby escape destruction at the hands of this bacterial adaptive immune system. Since their discovery, 36 distinct Acr families have been identified, including inhibitors for Cas proteins that are progressing to clinical use, such as SpyCas9, *S. aureus* Cas9 (SaCas9), and Cas12 (Cpf1) (for reviews of Acr families and inhibition mechanisms, see (Borges et al., 2017; Pawluk et al., 2017; Bondy-Denomy, 2018).

One example of an Acr protein with high potential as an affinity reagent is the SpyCas9 inhibitor, AcrIIA4. AcrIIA4 directly interacts with the DNA binding pocket of CRISPR/SpyCas9 RNP, binding to it with high specificity and affinity, thereby preventing the RNP from recognizing and cleaving its DNA sequence targets. We detail here our development of an engineered AcrIIA4 protein for use as an affinity reagent in a biosensing platform for detecting SpyCas9 and its RNP *via*, electrochemical, fluorescent, and colorimetric assays, the three most commonly utilized within research and/or clinical settings. Using this strategy, we demonstrate detection of SpyCas9 and its RNP in reaction buffer at picomolar levels, and in whole cell extracts with nanomolar sensitivity. More broadly, the highly specific interaction of Acr with its target CRISPR/Cas protein, facile production and scale up, and ease of Acr protein modification allowing for incorporation into bioassays, all represent significant advantages of Acr proteins as capture or detection ligands and demonstrate the potential of Acr proteins as alternatives to antibodies, facilitating development of robust platforms for CRISPR/Cas system detection, identification, and quantification.

2. Methods

2.1. Materials

All chemicals were purchased from MilliporeSigma (Burlington, MA) unless otherwise specified. SpyCas9, AcrIIA4, and fluorophore-/quencher-labeled deoxy oligonucleotides were obtained and purified as detailed in (Seamon et al., 2018). Antibodies (Abs) against the N-terminus (N-term; clone 7A9-3A3) or C-terminus (C-term; clone 6G12) of SpyCas9 (hereafter referred to as "Cas9"), and conjugated to horse radish peroxidase (HRP), were purchased from Novus Biologicals (Centennial, CO). HRP-conjugated anti-glucose oxidase (GOx) Abs were purchased from LifeSpan Biosciences (Seattle, WA). Pierce protein A/G beads were purchased from Thermo Fischer Scientific (Waltham, MA). All electrochemical measurements were conducted using a PalmSens hand-held potentiostat (Palm Instruments BV, The Netherlands) and a three-electrode electrochemical cell with glassy carbon working electrode (GCE), a platinum wire counter electrode and either a $Ag/AgNO_3$ (for nitrophenyl diazonium deposition) or 3M Ag/AgCl (for all other electrochemical measurements) reference electrode (Bioanalytical Systems, West Lafayette, IN).

2.2. Synthesis and purification of Cas9, sgRNA, and engineered AcrIIA4 (e-AcrIIA4)

Cas9 and sgRNA were synthesized and purified as described in (Seamon et al., 2018). AcrIIA4 was engineered to contain two cysteine groups and a hydrophilic linker, by using geneblocks to add an N-terminal Cys_2-$(GlyGlyGlyGlySer)_2$ sequence. This coding sequence was cloned into a pTXB1 vector (New England Biolabs, Ipswich, MA) and further outfitted with a C-terminal His_8 tag. This Cys_2-$(GlyGlyGlyGlySer)_2$-AcrIIA4-His_8 construct (hereafter referred to as "engineered AcrIIA4", or "e-AcrIIA4") was expressed in BL21(DE3) *E. coli*, and purified *via* Ni-NTA and anion exchange chromatography, as described previously for synthesis and purification of wild type (w.t.) AcrIIA4 (Seamon et al., 2018).

2.3. Generation of CRISPR/SpyCas9 RNP

CRISPR/SpyCas9 RNP (hereafter referred to as "RNP") was generated by mixing 200 nM Cas9 with 400 nM sgRNA in reaction buffer [20 mM Tris-HCl, pH 7.5, 100 mM NaCl, 5 mM $MgCl_2$, 0.1 mM EDTA] for 10 min at room temperature. A description of the *in-vitro* RNP activity assay, and its use to verify retained e-AcrIIA4 activity, is presented in the supplementary materials.

2.4. Formation of e-AcrIIA4 functionalized surfaces

Nitrophenyl thin films were electrodeposited onto clean GCEs (see supplemental material for electrode preparation procedure) from a solution of 1 mM nitrophenyl diazonium salt, 100 mM Bu_4NBF_4, in acetonitrile (ACN). For surface optimization experiments, three electrochemical protocols were used: Chronoamperometry (CA), linear sweep (LS), and cyclic voltammetry (CV). Following film deposition, GCE were sonicated in ACN for 30 seconds and washed with ethanol to remove unbound diazonium. Nitrophenyl groups were converted to aminophenyl groups by electrochemical treatment (2 CVs, -0.350 V to -1.3 V, scan rate, $\nu = 100\ \text{mV} \cdot \text{s}^{-1}$) in an ethanol:water solution (1:9) with 0.1 M KCl as electrolyte. Electrodes were then rinsed in water, dried under N_2, and immersed in 5 mM solution of the heterobifunctional crosslinker sulfo-EMCS, with 5 mM EDTA in 1 × PBS, pH 7.3, for 1 h. Electrodes were rinsed twice with 1 × PBS (pH 7.3, 5 mM EDTA), and then treated with 100 μM e-AcrIIA4 in 1 × PBS pH 7.3, 5 mM EDTA for 2–4 h. The resultant e-AcrIIA4 functionalized electrodes were then rinsed twice with 1 × PBS, pH 7.3.

2.5. Electrochemical, fluorescent and colorimetric detection of Cas9 using e-AcrIIA4

e-AcrIIA4 modified GCEs were incubated with analytes (Cas9, RNP, or GOx) in reaction buffer, or in RAW264.7 whole cell extracts, for 2 h. The GCE surfaces were then rinsed twice with 1 × PBS pH 7.3.

For electrochemical measurements, the GCE surfaces were further incubated with 30 μL HRP-conjugated anti-Cas9 N-term or C-term Abs (1:500 dilution in peroxidase stabilizer solution, Surmodics Eden Prairie, MN) for 45 min at room temperature. The GCE surfaces were then rinsed twice with 1 × PBS, pH 7.3, and immersed in TMB conductivity solution (Surmodics, Eden Prairie, MN) for electrochemical analysis.

For fluorescence measurements, the GCE surfaces were further incubated with 30 μL AlexaFluor488-conjugated anti-Cas9 N-term Abs for 45 min at room temperature. The GCE surfaces were then rinsed twice with 1 × PBS, pH 7.3, and imaged on an inverted epi-fluorescence microscope (Zeiss Axiovert 200M, Oberkochen, Germany) equipped with a monochrome high-resolution camera (Zeiss AxioCam HRm). All image analysis was performed using ImageJ 1.52a software (National Institutes of Health, USA). Fluorescence signal was quantified by identifying fluorescent puncta in 8-bit greyscale data sets by manually thresholding the image (2 × above the average background signal; threshold values were typically 26–30), and then summing the average intensities of the identified fluorescent puncta.

For colorimetric measurements, the GCE surfaces were further incubated with HRP-conjugated anti-Cas9 N-term Abs for 45 min at room temperature. The GCE surfaces were then rinsed twice with 1 × PBS, pH 7.3, incubated with 200 μL TMB conductivity solution for 2 min, and then removed. The solution was imaged using a Pixel 2 XL camera (12.2 Mega pixels f/1.8, 1.4 μm pixels, HTC, Taiwan).

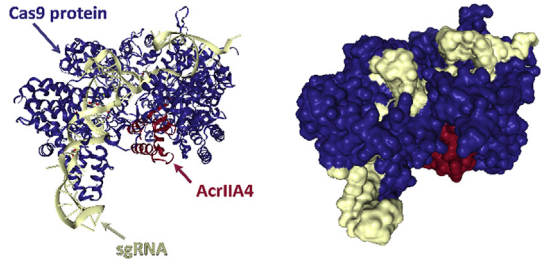

Engineered AcrIIA4: CC(GGGGS)2 AcrIIA4

CCGGGGSGGGGSMNINDLIREIKNKDYTVKLSGTDSNSITQLII
RVNNDGNEYVISESENESIVEKFISAFKNGWNQEYEDEEEFYN
DMQTITLKSELN

Cysteine (thiol group) Spacer/linker sequence

Fig. 1. Structure of AcrIIA4 (red) bound to RNP (Cas9, blue; plus sgRNA, white) illustrated by ribbon (left) and space-fill (right) models. The amino acid sequence of AcrIIA4 engineered with a spacer/linker sequence and two thiol handles ("e-AcrIIA4") is shown (bottom). (For interpretation of the references to color in this figure legend, the reader is referred to the Web version of this article.)

2.6. Preparation of RNP spiked whole cell extract (WCE) samples

RAW264.7 cells were cultured in DMEM supplemented with 10% (v/v) fetal bovine serum (FBS) and 1% (v/v) penicillin/streptomycin solution, in tissue culture treated flasks at 37 °C with 5% CO_2. Cells were harvested in approximately 200 µL of lysis buffer (20 mM HEPES, pH 7.5, 100 mM KCl, 5 mM $MgCl_2$, 5% glycerol, 0.1% Triton X-100, supplemented with Holt protease inhibitor cocktail), agitated for 20 min at 4 °C, and clarified *via* centrifugation. To the supernatant (whole cell extract; WCE), 200 nM Cas9 and 400 nM sgRNA were added, followed by incubation for 15 min at room temperature. RNP was subsequently diluted to the desired concentration using WCE.

3. Results & discussion

3.1. Engineering AcrIIA4 for use as an affinity reagent

As shown in Fig. 1 (Protein Data Bank entry 5VW1 (Yang and Patel, 2017),), the AcrIIA4 protein (red) binds within the protospacer adjacent motif (PAM) recognition site of the RNP (blue). This blocks binding and scanning of DNA sequences, preventing the RNP from recognizing target DNA (Dong et al., 2017; Yang and Patel, 2017; Kim et al., 2018). To utilize AcrIIA4 as an affinity reagent, the protein was engineered with two cysteines (Fig. 1, orange), providing thiol groups that can be used as a handle for AcrIIA4 immobilization *via* standard protein crosslinking chemistries. The protein was further modified with a 10-amino acid linker sequence, $(GlyGlyGlyGlySer)_2$, inserted between the AcrIIA4 protein and the cysteine handle (Fig. 1, green). This linker assists in maintaining the protein's conformational requirements (*e.g.*, structure, flexibility, separation from surface), facilitating interactions between the immobilized engineered AcrIIA4 (e-AcrIIA4) and the RNP suspended in solution.

3.2. e-AcrIIA4 generation and surface immobilization

AcrIIA4 has been reported to have exceptional specificity and affinity for the *S. pyogenes* CRISPR/Cas9 RNP (RNP), functioning as a mimic of the target DNA, making AcrIIA4 a promising affinity reagent. We engineered wild type AcrIIA4 with a hydrophilic spacer tail containing dual cysteine groups (e-AcrIIA4; see Fig. 1 and discussion in the supporting information) and verified the modified protein maintained RNP inhibiting ability using a FRET-based DNA cleavage activity assay (see Fig. S1 and discussion in the supporting information). e-AcrIIA4 was then immobilized onto a robust, well defined, conducting surface formed *via* aryl diazonium salt electrodeposition (Fig. 2), to facilitate RNP detection using standard bioanalytical techniques (electrochemical, fluorescent, and colorimetric). Electrode functionalization steps were confirmed using cyclic voltammetry with a redox probe (see Fig. S2 and discussion in the supporting information). Optimization of the electrodeposited surface for RNP detection is detailed in the supporting information and presented in Fig. S3.

3.3. RNP detection with surface-immobilized e-AcrIIA4

To characterize the ability of surface-immobilized e-AcrIIA4 to serve as an affinity reagent for RNP detection, e-AcrIIA4 functionalized GCE surfaces were incubated with RNP, followed by incubation with probes that enable electrochemical, fluorescent, or colorimetric detection.

For electrochemical detection, HRP-conjugated anti-Cas9 Abs were used as the probe. As shown in Fig. 3A, in a solution of TMB (3,3′,5,5′-tetramethybenzidine) mediator and H_2O_2 substrate, HRP catalytic turnover increases the relative concentration of oxidized TMB to reduced TMB. This results in a decrease in oxidation current measured at the electrode surface, and an increase in reduction current. This characteristic electrocatalytic behavior is shown in Fig. 3B. An e-AcrIIA4 functionalized electrode treated with buffer (negative control), followed by the HRP-conjugated anti-Cas9 Abs (probe), shows a near-Nernstian response typical of the TMB/H_2O_2 solution at a thin film modified surface (black trace). Electrodes treated with 300 nM RNP, followed by the HRP-Ab probe, showed a significant decrease in the TMB oxidation peak current ($E_{p,a}$ = 385 mV), with an increase in the TMB reduction peak current ($E_{p,c}$ = 235 mV), and a shifting of the reduction peak to more negative potentials (Fig. 3B, green and red traces). This indicates that HRP is present on the electrode surface, and that immobilized e-AcrIIA4 was able to interact with, bind to, and capture the RNP suspended in solution. These results demonstrate that Acr proteins can serve as affinity reagents for detection of their cognate RNPs.

In the experiment presented in Fig. 3B, two different HRP-conjugated anti-Cas9 Abs were used as probes: One targeting the Cas9 N-term (red trace), the other targeting the C-term (green). Exposure of the e-AcrIIA4 surface to RNP, followed by probing with anti-Cas9 C-term Abs, led to an 13% reduction in the oxidation wave peak current compared to the negative control (Fig. 3C, green bar). In contrast, probing with anti-Cas9 N-term Abs led to a much stronger decrease in

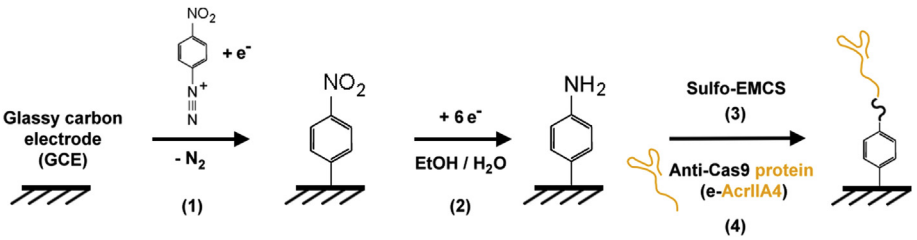

Fig. 2. Functionalization of a conductive surface with e-AcrIIA4. (1) Electroreduction of nitrophenyl diazonium, with subsequent loss of dinitrogen, and covalent grafting of the phenyl radical to the substrate. (2) Nitrophenyl groups are electrochemically reduced to aminophenyl groups under protic conditions. (3) A heterobifunctional crosslinker, sulfo-EMCS, is used to couple the surface bound aminophenyl groups to (4) thiol moieties (cysteines) on e-AcrIIA4.

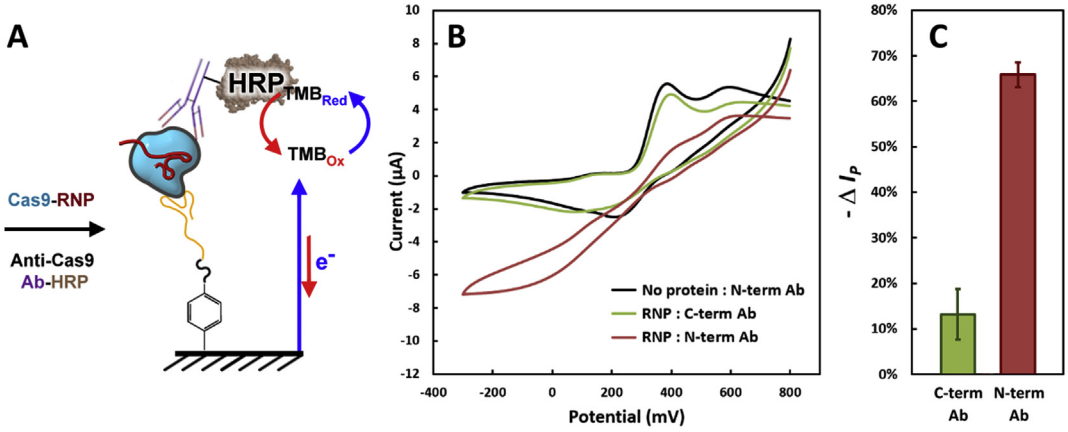

Fig. 3. RNP detection at an e-AcrIIA4 immobilized surface. (A) Capture of RNP and detection *via* an electroactive label (HRP) resulting in an electrocatalytic increase in TMB mediator reduction current, and a decrease in TMB oxidation current. (B) Cyclic voltammograms of e-AcrIIA4 immobilized electrodes exposed to: No protein + HRP-conjugated anti-Cas9 N-term Abs (black trace, negative control), 300 nM RNP + HRP-conjugated anti-Cas9 C-term Abs (green trace), or 300 nM RNP + HRP-conjugated anti-Cas9 N-term Abs (red trace). TMB/H_2O_2 solution, potential *vs.* Ag/AgCl, $\nu = 20\,mV \cdot s^{-1}$. (C) Plot of the decrease in TMB oxidation current peak height ($-\Delta I_p$) for surfaces probed with anti-Cas9 C-term Abs (green) or N-term Abs (red) *vs.* the no-protein control from panel (B). Error bars are the standard deviation of three replicates. (For interpretation of the references to color in this figure legend, the reader is referred to the Web version of this article.)

oxidative current compared to the negative control (66%; Fig. 3C, red bar). Several studies focusing on characterization of the interaction between AcrIIA4 and RNP have concluded that AcrIIA4 binds to RNP at three separate locations, one of which is the Cas9 C-term domain (Dong et al., 2017; Shin et al., 2017; Yang and Patel, 2017; Kim et al., 2018; Li et al., 2018). Therefore, this difference in catalytic activity measured using the C-term *versus* N-term Abs likely results from binding of e-AcrIIA4 to the C-terminal domain of the Cas9-RNP. This then inhibits anti-C-term Cas9 Abs from binding to the immobilized RNP. (Dong et al., 2017; Shin et al., 2017; Yang and Patel, 2017; Kim et al., 2018; Li et al., 2018). Given this result, all subsequent experiments were conducted using the anti-Cas9 N-term Abs as the detection probe.

3.4. Electrochemical, fluorescent, and colorimetric detection of RNP using e-AcrIIA4

Electrochemical, fluorescent and colorimetric-based detection of RNP at e-AcrIIA4 immobilized surfaces, and the signal dependence on RNP concentration, is presented in Fig. 4. Cyclic voltammograms at electrodes treated with different concentrations of RNP (0 pM–1 μM) are shown in Fig. 4A. The corresponding decrease in the TMB oxidative peak current is plotted in Fig. 4B. A dynamic range of 2 orders of magnitude was observed, with signal saturating at RNP concentrations near 250 nM. The limit of detection (LOD) was defined as the lowest signal of a positive control whose signal strength was greater than the sum of the mean signal of a negative control sample (μ), and its standard deviation (σ) multiplied by 5 (LOD = μ + 5σ). For electrochemical measurements, the LOD was 280 pM, which is similar to other enzymatically labeled electrochemical assays (Freitas et al., 2019). The dynamic range is somewhat narrow; however, the range is suitable for detecting Cas9-RNP at concentrations relevant to gene editing applications with potential clinical relevancy. As an example, a recent study by Lee and coworkers (Lee et al., 2017) demonstrated gene editing and repair in cell models of muscular dystrophy by delivering 8 μg/mL (50 nm) of Cas9, a concentration well within the dynamic range of this AcrIIA4-based electrochemical detection platform.

Use of surface-immobilized e-AcrIIA4 as an affinity reagent for fluorescent measurement is presented in Fig. 4C and D. Anti-Cas9 N-term Abs conjugated to Alexa Fluor 488 (Abs-AF488) were used as the detection probe, and the GCE surface was imaged using an inverted epi-fluorescence microscope equipped with a custom-made fixture for mounting electrodes. Fluorescence images of an e-AcrIIA4 functionalized GCE surface (only), an e-AcrIIA4 surface probed with Abs-AF488 (no RNP), and an e-AcrIIA4 surface exposed to a non-RNP target protein at high concentration (glucose oxidase, GOx; 10 μM) followed by probing with Abs-AF488, each showed no fluorescent signal (Fig. 4C, top panel), indicating no detectable non-specific binding of Abs-AF488 or auto-fluorescence from e-AcrIIA4. Exposure of the e-AcrIIA4 modified GCE surfaces to RNP at eight different concentrations, ranging from 0 pM to 1 μM, followed by probing with Abs-AF488, resulted in strong and concentration-dependent fluorescent signals (Fig. 4C, bottom panel). Fluorescent signals were quantified using ImageJ 1.52a software, and results are shown in Fig. 4D. A narrower dynamic range of 1.25 orders of magnitude, and a higher LOD of 3 nM, were observed in comparison to the electrochemical detection method. These results are consistent with other reports that electrochemical assays generally exhibit one or more orders of magnitude lower LODs than similar fluorescence-based bioanalytical assays (Raj et al., 2007; Zhang et al., 2017).

To assess the colorimetric detection capability of an e-AcrIIA4 modified surface, electrodes exposed to RNP were probed with HRP-conjugated anti-Cas9 N-term Abs and then immersed in TMB/H_2O_2 solution for 2 min in microcentrifuge tubes; the electrodes were then removed, and the microcentrifuge tubes imaged (see Fig. 4E). HRP turnover in the TMB/H_2O_2 solution generates a blue product (cation free oxidized TMB radical). Within the 2-min reaction time, the HRP turnover product was clearly visible from electrodes treated with 10 nM or greater concentrations of RNP (Fig. 4E). Increasing amounts of the blue product were observed when the TMB/H_2O_2 solution was incubated with electrodes exposed to higher concentrations of RNP; however, this unoptimized colorimetric assay is only roughly quantitative.

3.5. Specificity and robustness of e-AcrIIA4 mediated detection of RNP

The specificity of surface immobilized e-AcrIIA4 and its performance in relevant sample matrices was evaluated. To assess specificity, the reduction in TMB oxidation peak was measured for electrodes exposed to GOx (a non-target protein of molecular weight similar to Cas9), Cas9 (without sgRNA), or RNP, followed by probing with HRP-conjugated Abs against either GOx or Cas9 (N-term). As shown in Fig. 5A, GCEs exposed to GOx and probed with either anti-Cas9 or anti-GOx Abs showed a minimal decrease in oxidative peak current of 5% (Fig. 5A, light red) or 7% (Fig. 5A, dark red), respectively. These results are consistent with the fluorescence detection results presented in Fig. 4C, and those of other studies which have found that non-specific

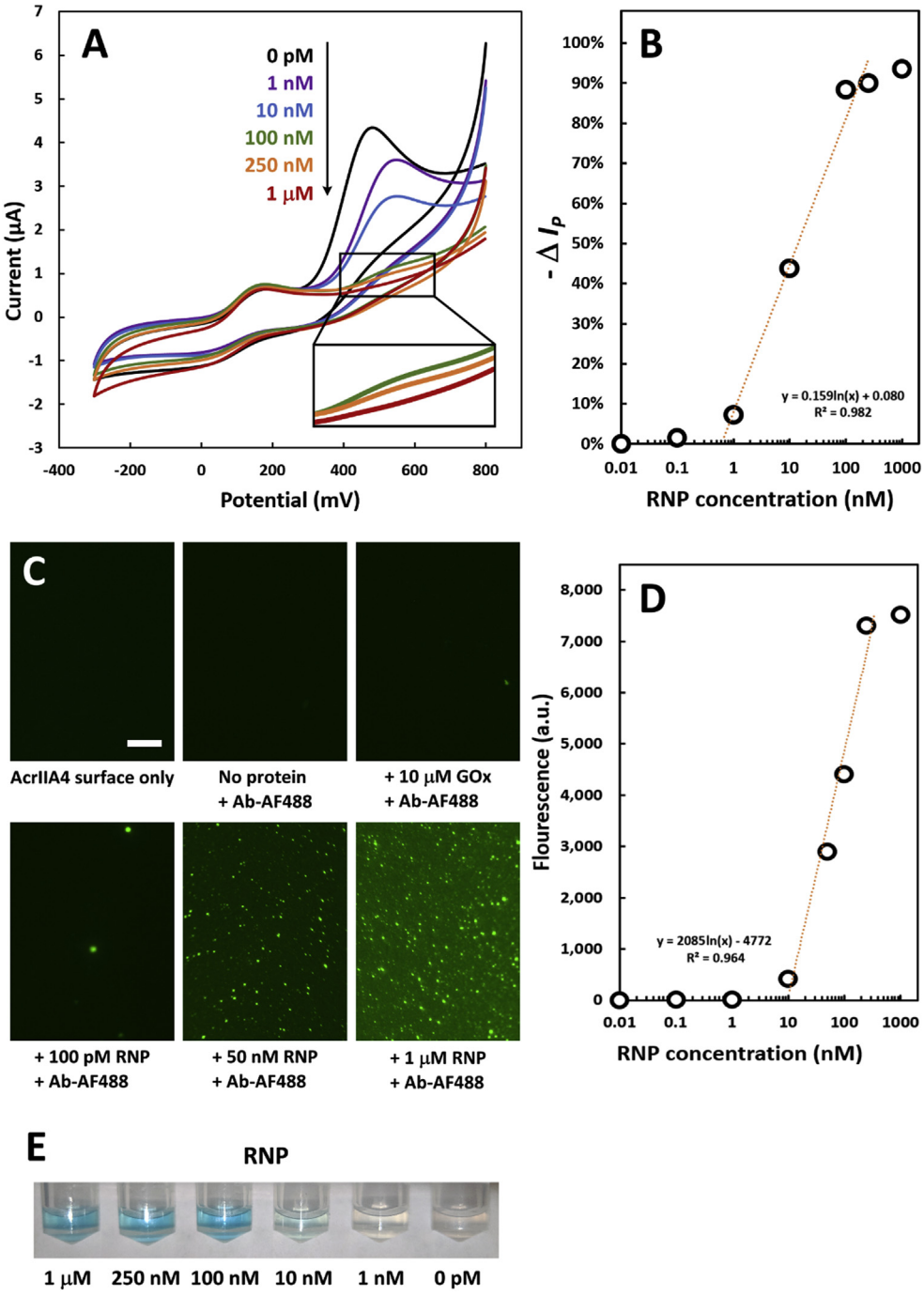

Fig. 4. Electrochemical, fluorescent, and colorimetric detection of RNP using immobilized e-AcrIIA4 as an affinity reagent. (A) Cyclic voltammograms (CVs) from e-AcrIIA4 modified GCEs exposed to varying concentrations of RNP. TMB/H_2O_2 solution, potential *vs.* Ag/AgCl, $\nu = 20\,mV \cdot s^{-1}$. (B) Impact of RNP concentration on current response (decease in TMB oxidation peak, $-\Delta I_p$). (C) Fluorescence microscopy images of e-AcrIIA4 immobilized GCE surfaces treated with no protein, GOx or RNP, followed by incubation with AF488-conjugated Abs. All images were captured under identical magnification and camera settings, and are false colored. Scale = 20 μm. (D) Fluorescence intensity following treatment with varying RNP concentrations. (E) Photograph of microcentrifuge tubes containing TMB/H_2O_2 solution following a 2-min exposure to e-AcrIIA4 immobilized GCEs treated with RNP and incubated with HRP-conjugated anti-Cas9 N-term Abs.

binding typically generates responses of < 10% in similar affinity-based electrochemical bioassays (Pil et al., 2010; Hwang et al., 2017; Lim et al. 2017, 2018). We conclude that the HRP-conjugated Abs (anti-GOx and anti-Cas9 N-term), as well as the non-cognate protein used as a negative control (GOx), show only marginal non-specific binding to the e-AcrIIA4 modified surface.

e-AcrIIA4 modified GCE surfaces exposed to Cas9 or RNP and probed with anti-GOx Abs showed an 18% (Fig. 5A, light blue) and 12% (Fig. 5A, light green) decrease in oxidation current, respectively, indicating that the Cas9-/RNP-bound protein layers increase non-specific interactions with the non-cognate probe (anti-GOx Abs). This may be due to the differing electrostatic interactions and conformational flexibility for Cas9 *versus* RNP. The high pI of Cas9 (pI = 8.9–9.0) makes it positively charged at the assay pH, whereas RNP has an overall negative charge imparted by the sgRNA. It is possible that electrostatic interactions between positively charged Cas9 and AcrIIA4, which is negatively charged at the assay pH (w.t. pI = 4.1), promote increased surface binding of Cas9 relative to RNP. Additionally, Cas9 has been shown to have much more conformational flexibility than RNP (Shibata et al., 2017). However, this non-specific binding signal is still quite low as compared to the 80% (Fig. 5A, dark blue) and 52% (Fig. 5A, dark green) decrease in oxidation current obtained from Cas9 or RNP exposure (respectively) followed by probing with anti-Cas9 Abs, underscoring the specificity with which the e-AcrIIA4 modified surface binds Cas9 and RNP.

The stronger response from e-AcrIIA4 modified electrodes exposed to Cas9, as compared to those exposed to RNP (Fig. 5A), was unexpected, given that a recent study found that AcrIIA4 binds to RNP with approximately 8000-fold greater affinity than to Cas9 (Kim et al., 2018). It is possible that the observed stronger response to Cas9 was

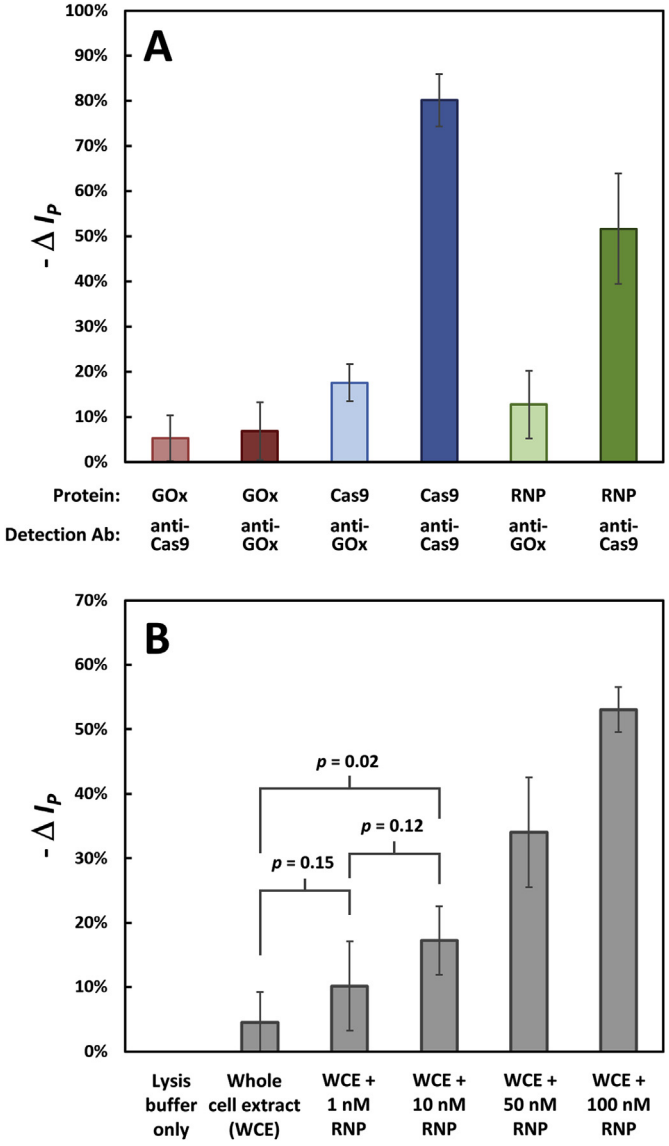

Fig. 5. Specificity and robustness of e-AcrIIA4 mediated detection of RNP. (A) Change in TMB oxidation current response (-Δ*Ip*) upon exposure to 50 nM GOx, Cas9 (without sgRNA), or RNP and probed with either HRP-conjugated anti-GOx or anti-Cas9 Abs. (B) Change in TMB oxidation current response for e-AcrIIA4-modified electrodes exposed to lysis buffer, RAW264.7 whole cell extract (WCE), or WCE containing varying concentrations of RNP. Error bars indicate the standard deviation of three replicate assays.

due to a difference in AcrIIA4 conformation introduced upon incorporation of linker sequence and/or immobilization on a surface. Also, given the potentially favorable electrostatic interactions between Cas9 and AcrIIA4 modified surfaces mentioned above, any change or restriction in AcrIIA4 confirmation could increase binding affinity of Cas9 to AcrIIA4. Additionally, a difference in the specificity of the detection probe (anti-Cas9 Abs) in recognizing Cas9 *versus* RNP could be responsible for the observed effect. Consistent with this last possibility, in immunoprecipitation (IP) experiments performed using anti-Cas9 N-term Abs, Cas9 was depleted from reaction supernatants to a much greater extent than was RNP (Fig. S4), indicating that the anti-Cas9 N-term Abs bind to Cas9 with higher affinity than to RNP. This result is not unexpected, given that the Abs were produced against Cas9 and not RNP. Further optimization of the binding conditions or detection antibodies, perhaps by targeting Cas9 regions that become more exposed upon sgRNA binding, might improve specificity for RNP, potentially facilitating quantification of RNP/Cas9 ratios in complex samples.

To assess the ability of immobilized e-AcrIIA4 to enable specific detection of RNP in a complex sample matrix, whole cell extracts (WCEs) were generated from RAW264.7 cells and spiked with varying amounts of RNP. The current responses from these samples are presented in Fig. 5B. No current response was obtained from electrodes exposed to lysis buffer, and a reduction in current response of 5% was observed from electrodes exposed to WCE without RNP, indicating a similar level of non-specific binding as observed upon electrode exposure to GOx. In contrast, electrodes exposed to WCEs containing increasing concentrations of RNP showed commensurate increases in current response (-Δ*Ip*), though the LOD in WCE (9 nM) was not as low as that in reaction buffer (*e.g.* *p*-value of 0.15 for WCE only *versus* WCE +1 nM RNP). This is not unexpected as higher LODs are typical when using complex sample matrices. Overall, these results demonstrate the ability of e-AcrIIA4 to serve as a capture ligand for detection of Cas9 and RNP in a relevant and complex sample matrix. We further demonstrate that the engineered anti-CRISPR protein AcrIIA4 is similar, by way of detection limit and specificity, to antibody-based electrochemical detection (Fig. S5).

4. Conclusion

In summary, our studies demonstrate the potential of anti-CRISPR (Acr) proteins as affinity reagents for detection of CRISPR/Cas systems in bioanalytical platforms. We incorporated a di-cysteine linker into the SpyCas9 anti-CRISPR protein AcrIIA4, which facilitated protein attachment to glassy carbon electrodes while maintaining the AcrIIA4 protein's ability to bind and inhibit (and therefore recognize) SpyCas9-RNP. Using AcrIIA4 modified electrodes in combination with HRP- and AlexaFluor-conjugated anti-Cas9 Abs, we demonstrated electrochemical, fluorescent, and colorimetric detection of picomolar concentrations of RNP in buffer and, more importantly, nanomolar concentrations in WCEs, demonstrating that AcrIIA4 can serve as an affinity reagent in bioanalytical assays with potential for analysis of samples drawn from basic and clinical research. To our knowledge, this is the first study demonstrating use of immobilized AcrIIA4 as an affinity reagent for detection of RNP *via* electrochemical, fluorescent, or colorimetric assays. This work, along with a recent report using a broad spectrum Acr (AcrIIC1) for microfluidic detection of diverse CRISPR/Cas components (Phaneuf et al., 2019), paves the way for future development of bioanalytical platforms that integrate newly-discovered Acr proteins as affinity reagents for highly specific and sensitive detection of gene editing components in complex sample matrices.

Declaration of interests

The authors declare that they have no known competing financial interests or personal relationships that could have appeared to influence the work reported in this paper.

CRediT authorship contribution statement

Robert K. Johnston: Conceptualization, Data curation, Investigation, Writing - original draft. **Kyle J. Seamon:** Data curation, Investigation, Resources, Supervision, Writing - review & editing. **Edwin A. Saada:** Data curation, Investigation, Resources, Supervision, Writing - review & editing. **Joshua D. Podlevsky:** Data curation, Investigation, Resources, Supervision, Writing - review & editing. **Steven S. Branda:** Writing - review & editing, Project administration, Supervision, Funding acquisition. **Jerilyn A. Timlin:** Writing - review & editing, Project administration, Supervision, Funding acquisition. **Jason C. Harper:** Conceptualization, Data curation, Investigation, Writing - original draft.

Acknowledgements

This work was supported by the DARPA Safe Genes program (K.J.S; E.A.S), and the Laboratory Directed Research and Development program at Sandia National Laboratories (R.K.J; J.P; S.S.B; J.A.T; J.C.H). Sandia National Laboratories is a multi-program laboratory managed and operated by National Technology and Engineering Solutions of Sandia, LLC., a wholly owned subsidiary of Honeywell International, Inc., for the U.S. Department of Energy's National Nuclear Security Administration under contract DE-NA-0003525.

Appendix A. Supplementary data

Supplementary data to this article can be found online at https://doi.org/10.1016/j.bios.2019.111361.

References

Barrangou, R., Marraffini, L.A., 2014. CRISPR-cas systems: prokaryotes upgrade to adaptive immunity. Mol. Cell 54 (2), 234–244.
Barrangou, R., Fremaux, C., Deveau, H., Richards, M., Boyaval, P., Moineau, S., Romero, D.A., Horvath, P., 2007. CRISPR provides acquired resistance against viruses in prokaryotes. Science 315 (5819), 1709–1712.
Bondy-Denomy, J., 2018. Protein inhibitors of CRISPR-cas9. ACS Chem. Biol. 13 (2), 417–423.
Bondy-Denomy, J., Pawluk, A., Maxwell, K.L., Davidson, A.R., 2013. Bacteriophage genes that inactivate the CRISPR/Cas bacterial immune system. Nature 493 (7432) 429-U181.
Borges, A.L., Davidson, A.R., Bondy-Denomy, J., 2017. The discovery, mechanisms, and evolutionary Impact of anti-CRISPRs. Annu. Rev. Virol. 4 (1), 37–59.
Charlesworth, C.T., Deshpande, P.S., Dever, D.P., Dejene, B., Gomez-Ospina, N., Mantri, S., Pavel-Dinu, M., Camarena, J., Weinberg, K.I., Porteus, M.H., 2018. Identification of Pre-existing Adaptive Immunity to Cas9 Proteins in Humans. bioRxiv.
Chew, W.L., 2018. Immunity to CRISPR Cas9 and Cas12a therapeutics. Wiley Interdisciplinary Reviews: Systems Biology and Medicine 10 (1) e1408.
Crudele, J.M., Chamberlain, J.S., 2018. Cas9 immunity creates challenges for CRISPR gene editing therapies. Nat. Commun. 9 (1), 3497.
Datsenko, K.A., Pougach, K., Tikhonov, A., Wanner, B.L., Severinov, K., Semenova, E., 2012. Molecular memory of prior infections activates the CRISPR/Cas adaptive bacterial immunity system. Nat. Commun. 3, 7.
Dong, D., Guo, M.H., Wang, S.H., Zhu, Y.W., Wang, S., Xiong, Z., Yang, J.Z., Xu, Z.L., Huang, Z.W., 2017. Structural basis of CRISPR-SpyCas9 inhibition by an anti-CRISPR protein. Nature 546 (7658), 436–+.
Freitas, M., Nouws, H.P.A., Delerue-Matos, C., 2019. Electrochemical sensing platforms for HER2-ECD breast cancer biomarker detection. Electroanalysis 31 (1), 121–128.
Hwang, H.J., Ryu, M.Y., Park, C.Y., Ahn, J., Park, H.G., Choi, C., Ha, S.-D., Park, T.J., Park, J.P., 2017. High sensitive and selective electrochemical biosensor: label-free detection of human norovirus using affinity peptide as molecular binder. Biosens. Bioelectron. 87, 164–170.
Jinek, M., Chylinski, K., Fonfara, I., Hauer, M., Doudna, J.A., Charpentier, E., 2012. A programmable dual-RNA-guided DNA endonuclease in adaptive bacterial immunity. Science 337 (6096), 816–821.
Kim, I., Jeong, M., Ka, D., Han, M., Kim, N.K., Bae, E., Suh, J.Y., 2018. Solution structure and dynamics of anti-CRISPR AcrIIA4, the Cas9 inhibitor. Sci. Rep. 8, 9.
Lee, K., Conboy, M., Park, H.M., Jiang, F., Kim, H.J., Dewitt, M.A., Mackley, V.A., Chang, K., Rao, A., Skinner, C., Shobha, T., Mehdipour, M., Liu, H., Huang, W.-c., Lan, F., Bray, N.L., Li, S., Corn, J.E., Kataoka, K., Doudna, J.A., Conboy, I., Murthy, N., 2017. Nanoparticle delivery of Cas9 ribonucleoprotein and donor DNA in vivo induces homology-directed DNA repair. Nat. Biomed. Eng. 1 (11), 889–901.
Li, J., Xu, Z.L., Chupalov, A., Marchisio, M.A., 2018. Anti- CRISPR-based biosensors in the yeast S. cerevisiae. J. Biol. Eng. 12, 14.
Lim, J.M., Ryu, M.Y., Yun, J.W., Park, T.J., Park, J.P., 2017. Electrochemical peptide sensor for diagnosing adenoma-carcinoma transition in colon cancer. Biosens. Bioelectron. 98, 330–337.
Lim, J.M., Kim, J.H., Ryu, M.Y., Cho, C.H., Park, T.J., Park, J.P., 2018. An electrochemical peptide sensor for detection of dengue fever biomarker NS1. Anal. Chim. Acta 1026, 109–116.
Pattanayak, V., Lin, S., Guilinger, J.P., Ma, E., Doudna, J.A., Liu, D.R., 2013. High-throughput profiling of off-target DNA cleavage reveals RNA-programmed Cas9 nuclease specificity. Nat. Biotechnol. 31, 839.
Pawluk, A., Bondy-Denomy, J., Cheung, V.H.W., Maxwell, K.L., Davidson, A.R., 2014. A new group of phage anti-CRISPR genes inhibits the type I-E CRISPR-cas system of Pseudomonas aeruginosa. mBio 5 (2), 7.
Pawluk, A., Davidson, A.R., Maxwell, K.L., 2017. Anti-CRISPR: discovery, mechanism and function. Nat. Rev. Microbiol. 16, 12.
Phaneuf, C.R., Seamon, K.J., Eckles, T.P., Sinha, A., Schoeniger, J.S., Harmon, B., Meagher, R.J., Abhyankar, V.V., Koh, C.-Y., 2019. Ultrasensitive multi-species detection of CRISPR-Cas9 by a portable centrifugal microfluidic platform. Anal. Method. 11 (5), 559–565.
Pil, P.J., C.D.M., Scott, B., 2010. High affinity peptides for the recognition of the heart disease biomarker troponin I identified using phage display. Biotechnol. Bioeng. 105 (4), 678–686.
Raj, V., Hari, P.R., Sreenivasan, K., 2007. Use of chemically modified thermoresponsive copolymers for the detection of C-reactive protein. Anal. Chim. Acta 592 (1), 45–50.
Seamon, K.J., Light, Y.K., Saada, E.A., Schoeniger, J.S., Harmon, B., 2018. Versatile high-throughput fluorescence assay for monitoring Cas9 activity. Anal. Chem. 90 (11), 6913–6921.
Shibata, M., Nishimasu, H., Kodera, N., Hirano, S., Ando, T., Uchihashi, T., Nureki, O., 2017. Real-space and real-time dynamics of CRISPR-Cas9 visualized by high-speed atomic force microscopy. Nat. Commun. 8 (1), 1430.
Shin, J., Jiang, F.G., Liu, J.J., Bray, N.L., Rauch, B.J., Baik, S.H., Nogales, E., Bondy-Denomy, J., Corn, J.E., Doudna, J.A., 2017. Disabling Cas9 by an anti-CRISPR DNA mimic. Sci. Adv. 3 (7), 9.
Wagner, D.L., Amini, L., Wendering, D.J., Burkhardt, L.-M., Akyüz, L., Reinke, P., Volk, H.-D., Schmueck-Henneresse, M., 2019. High prevalence of Streptococcus pyogenes Cas9-reactive T cells within the adult human population. Nat. Med. 25, 242–248.
Yang, H., Patel, D.J., 2017. Inhibition mechanism of an anti-CRISPR suppressor AcrIIA4 targeting SpyCas9. Mol. Cell 67 (1), 117–+.
Zhang, J., Zhang, W., Guo, J., Wang, J., Zhang, Y., 2017. Electrochemical detection of C-reactive protein using Copper nanoparticles and hybridization chain reaction amplifying signal. Anal. Biochem. 539, 1–7.